

# Spatially sculpted laser scissors for study of DNA damage and repair

**Jared Stephens**  
**Samarendra K. Mohanty**  
**Suzanne Genc**

University of California, Irvine  
Beckman Laser Institute and Medical Clinic  
1002 Health Sciences Road East  
Irvine, California 92617

**Xiangduo Kong**  
**Kyoko Yokomori**

University of California, Irvine  
School of Medicine  
Department of Biological Chemistry  
240D Med Sci I  
Irvine, California 92697

**Michael W. Berns**

University of California, Irvine  
Beckman Laser Institute and Medical Clinic  
1002 Health Sciences Road East  
Irvine, California 92617  
and  
University of California, Irvine  
Department of Biomedical Engineering  
3120 Natural Sciences II  
Irvine, California 92697

## 1 Introduction

Over the past several decades, laser scissors have proven an invaluable tool for microdissection in cell and developmental biology.<sup>1</sup> Through their continual refinement, a high level of precision in single-cell manipulation has been achieved. Noteworthy cellular applications of optical scissors include the ablation of axons,<sup>2</sup> microtubules,<sup>3,4</sup> and chromosomes,<sup>5-7</sup> as well as plasma membrane poration.<sup>8</sup> Recently, optical scissors have seen extensive use in DNA damage repair research by exposing a linear path across the nucleus of interphase cells followed by the monitoring of DNA damage recognition and repair in the altered region.<sup>9-15</sup>

Current approaches to laser-induced linear DNA damage consist primarily of moving the sample back and forth under a stationary focused laser beam via the microscope stage (motorized or manual), or moving the beam via a fast-scanning galvomirror (FSM) placed in the beam path (Fig. 1). In both cases of scanning, linear DNA damage is possible, but certain practical limitations exist when an area of damage that extends beyond the diffraction limited spot is desired. In cases where the microscope stage is moved, damage occurs to a greater degree on the edges of the linear path due to the lag time associated with changing the stage direction (when repeated paths over the same cell region are necessary), as well

**Abstract.** We present a simple and efficient method for controlled linear induction of DNA damage in live cells. By passing a pulsed laser beam through a cylindrical lens prior to expansion, an elongated elliptical beam profile is created with the ability to expose controlled linear patterns while keeping the beam and the sample stationary. The length and orientation of the beam at the sample plane were reliably controlled by an adjustable aperture and rotation of the cylindrical lens, respectively. Localized immunostaining by the DNA double strand break (DSB) markers phosphorylated H2AX ( $\gamma$ H2AX) and Nbs1 in the nuclei of HeLa cells exposed to the "line scissors" was shown via confocal imaging. The line scissors method proved more efficient than the scanning mirror and scanning stage methods at induction of DNA DSB damage with the added benefit of having a greater potential for high throughput applications. © 2009 Society of Photo-Optical Instrumentation Engineers. [DOI: 10.1117/1.3213601]

Keywords: laser microbeam; spatially sculpted scissors; DNA damage.

Paper 09109R received Mar. 25, 2009; revised manuscript received Jun. 9, 2009; accepted for publication Jul. 6, 2009; published online Sep. 22, 2009.

as when initiation and termination of stage movement are required. When an FSM is used to steer the beam, curvature at the edges of long linear cuts arises due to the steep angle to which the beam is reflected off the mirror surface.

Additionally, uniformity of damage production across a linear target zone may be difficult to achieve by both the stage moving and the FSM approaches since both methods utilize trains of pulses to damage the target material. Since the focal plane of the diffraction limited spot is circular, regions along a linearly exposed path may be exposed to overlapping pulses [Fig. 2(a)] or no pulses, all dependent on either the rate of the stage movement or the rate of the FSM movement. At though each can be minimized by tuning the distance between delivered pulses, minimization of one will result in exaggeration of the other. These variations make it difficult to compare damage in the exposed path from one experiment to the next.

In an attempt to improve the quality of focused laser-induced damage in living cells, we have developed an optical system that incorporates a cylindrical lens in the beam path coupled to an automated electronically controlled rotating mount and an automated iris. This optical system stretches the beam into a linear pattern and provides precise control over the length and radial orientation of the exposure pattern. By shaping the laser beam into a uniform linear pattern, it is possible to achieve a higher throughput of exposed cells, with an increased dosimetric uniformity and accuracy.

Address all correspondence to: Samarendra K. Mohanty, Beckman Laser Institute and Medical Clinic, University of California, Irvine, CA 92612. Tel: 949-824-7859; Fax: 949-824-8413; E-mail: smohanty@uci.edu

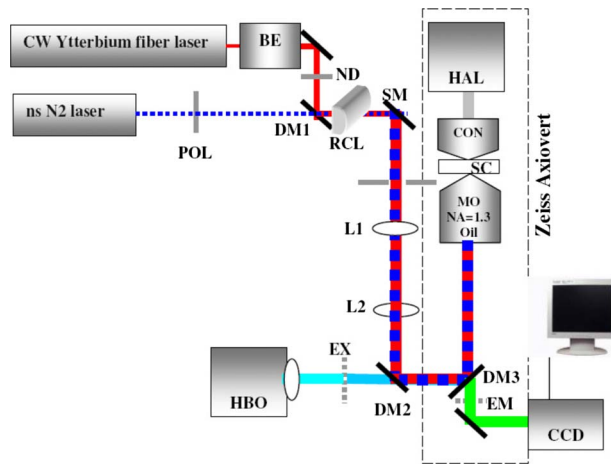


**Fig. 1** Schematic of line scissors and tweezers setup. POL: polarizer; BE: beam expander; M: folding mirror; ND: neutral density filter; DM1: dichroic mirror (reflects IR and transmits UV); RCL: rotatable cylindrical lens; SM: XY-scanning mirror; VAP: variable circular aperture; L1 and L2: 1:1 telescope; HBO: mercury lamp; EX: excitation filter; DM2: dichroic mirror (reflects UV and IR and transmits blue); DM3: dichroic mirror (reflects UV-blue and IR, but transmits green-red); MO: microscope objective; SC: sample chamber; CON: condenser; HAL: halogen lamp; EM: emission filter.

## 2 Materials and Method

### 2.1 Cell Culture

HeLa S3 cells obtained from American Type Culture Collection were cultured in Advanced DMEM F12 (GibcoBrl) media at 37 °C with 5% CO<sub>2</sub> supplementation. Cells were grown on gridded glass-bottomed imaging dishes (Matek). Prior to the experiments, growth media was replaced with media lacking phenol red to minimize light absorption by the media.

### 2.2 Set up

The experimental setup for the spatially sculpted line scissors is shown in Fig. 1. A pulsed N<sub>2</sub> laser (4 ns, 337 nm, 300 μJ/pulse, 75 kW peak pulse power, 1 to 60-Hz VSL-337ND-S, Spectra Physics, California) was linearly polarized (POL) and focused through a cylindrical lens (RCL) to an elliptical profile. A CW Ytterbium fiber laser (1070 nm, 20 W, PYL-20M, IPG Photonics, Oxford, Massachusetts) beam was collimated/expanded via a 6× beam expander, guided through a folding mirror (M), and aligned with the N<sub>2</sub> laser beam by use of a dichroic mirror (DM1) prior to being focused through the rotating cylindrical lens (RCL). The elliptic UV (and or IR) laser beam was relayed to the back aperture of the microscope objective (40× Zeiss Neofluar NA=1.3) via the epifluorescence port by use of 1:1 telescopic lens system (L1 and L2). The RCL was mounted on a motorized rotational stage, enabling control of radial orientation of the elliptic beam, and was secured by a flipping mount so that the system could toggle between spot and elliptical profiles depending on the desired application. A scanning mirror (SM) was placed in the beam path to enable scanning of the beam for applications where producing damage in multiple regions of interest (ROIs) are targeted. An electronically driven variable aperture (VAP) was placed at the focal plane of the cy-

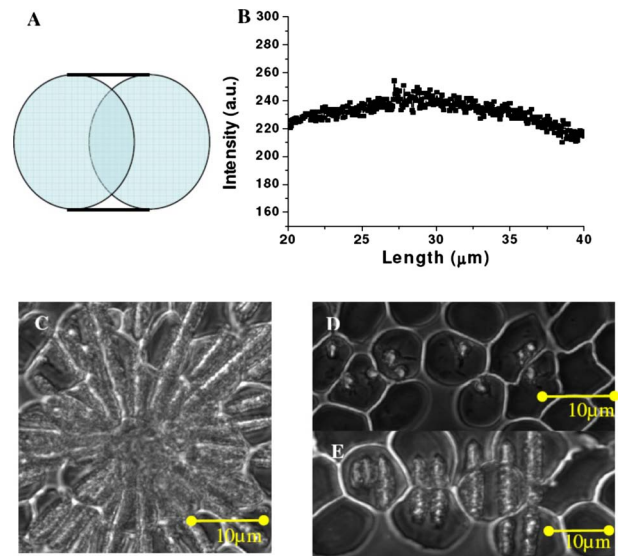


**Fig. 2** Control of line scissors dimension and orientation. (a) Illustration of the inherent variability in irradiance delivered to a linear ROI when using a diffraction-limited spot profile. The dark blue areas received greater than average total irradiance compared to the majority of the ROI, whereas the white areas bordered by light blue regions and dark lines represent areas that received little if any irradiance as compared to the majority of the ROI. (b) Intensity profile (along length) of the elliptically focused spot monitored by fluorescence; (c) line cuts on RBC in different radial orientations of the cylindrical lens; and (d) point and (e) controlled line cuts generated by varied restriction of the beam by the aperture. (Color online only.)

lindrical lens to govern the length of the focused beam. For fluorescence imaging, light from a mercury lamp (HBO) was coupled to the microscope through a dichroic mirror (DM2) that reflects UV and IR beams but transmits the visible region of the mercury spectrum. The excitation filter (EX) was placed in a filter wheel, and another dichroic mirror (DM3) was used to reflect the fluorescence excitation light, the 337-nm laser scissors beam, and the 1070-nm laser tweezers beam. DM3 transmitted the emitted fluorescence as well as the transmitted halogen (HAL) light from the sample in the sample chamber (SC). The emission filter (EM) blocked the 337-nm laser scissors and 1070-nm laser tweezers beams. Using the dual-objective method<sup>16</sup> the transmission factor of the objective for the 337-nm laser was determined to be 42%. The energy/pulse entering the back aperture of the objective was measured to be 0.1 μJ, giving a value of ~0.04 μJ at the sample plane.

The dimensions of the generated elliptical focused spot determine the length over which the object(s) can be ablated. Use of a 50-mm focal length cylindrical lens produces a focal spot length of ~40 μm at the object plane. The intensity variation along the length of the elliptically focused spot was monitored by dye fluorescence and is shown in Fig. 2(b). Although the overall beam profile (40 μm) is elliptical, we selected an even smaller (10 μm) central region with the aperture that was effectively linear for our experiments. Further, it may be noted that the actual intensity profile [in Fig. 2(b)] depends quadratically on intensity of excitation. Control of energy/pulse was achieved by orientation of a rotating polarizer (POL).

Discrete trains of pulses were delivered by using a data acquisition and control (DAQ) board (National Instruments) to activate an external trigger option on the laser. Ablation of air-dried red blood cells (RBCs) with the line scissors demonstrated the precision of the radial orientation [Fig. 2(c)] and length by sequential adjustments [Figs. 2(d) and 2(e)]. Figure 2(c) shows the achieved level of precision in control over orientation of the ROI by rotating the cylindrical lens in the motorized rotating mount (Thorlabs, Inc., Newton, NJ). Single pulses were delivered at 15 deg intervals over 180 deg of total rotation. Figure 2(d) shows the ROI constricted to a point cut, and Fig. 2(e) shows that the constricted ROI can easily be expanded to a linear form. For DNA damage repair experiments, the iris was used to limit the dimensions of the elongated beam at the sample plane to 10  $\mu\text{m}$ . The polarizer was then used to tune the pulse energy to 0.1  $\mu\text{J}$  at the back aperture of the objective. This provided a peak power density of  $0.033 \times 10^{10} \text{ W/cm}^2$  as compared to  $1 \times 10^{10} \text{ W/cm}^2$  for the focused spot used in parallel scanning stage and scanning mirror configuration experiments.<sup>17</sup>

### 2.3 Immunostaining

After damage induction, HeLa cells were fixed in 4% paraformaldehyde (PFA) for 10 min. A post fixation cytoplasmic extraction was then carried out with CSK buffer at 4 °C or for 5 min, as previously described.<sup>13</sup> Staining was conducted as previously described for phosphorylated H2AX ( $\gamma\text{H2AX}$ ) or Nbs1,<sup>12</sup> both of which are known to form ionizing radiation-induced foci (IRIF) around the double strand break (DSB) sites.<sup>18–22</sup> A minimum of five cells were irradiated per plate for three replicates.

### 2.4 Laser Scanning Confocal Microscopic Imaging

Confocal images were collected on a Zeiss Meta LSM 510. For each experiment, a Z-stack of 15  $\mu\text{m}$  was done with 1- $\mu\text{m}$  slices. Suitable dichroic mirrors and emission bandpass filters were configured for detection of Alexa-488 stained  $\gamma\text{H2AX}$  and Cy3 stained DNA repair factor (Nbs1) accumulation.

## 3 Results and Discussion

In order to determine the damage capabilities of the optical line scissors, the induction of DNA DSBs was assayed. Immediately following laser exposure, cells were fixed and immunostained for the phosphorylated H2AX ( $\gamma\text{H2AX}$ ) (Fig. 3).  $\gamma\text{H2AX}$  was selected because it is a well-accepted marker for DNA DSBs in mammalian cells<sup>18–20</sup> and produces prominent foci even where low levels of damage have occurred. Laser scanning confocal microscopic analysis of HeLa cells whose nuclei were exposed to the line-shaped scissors showed clear  $\gamma\text{H2AX}$  focus formation confined to the beam profile at dosimetry levels similar to other methods of laser-induced DNA damage (Fig. 3). From the Z-stack fluorescence reconstruction,  $\gamma\text{H2AX}$  fluorescence staining was observed over a cylinder with radius of 3  $\mu\text{m}$ .

One caveat of  $\gamma\text{H2AX}$  staining as a method of DSB detection is that  $\gamma\text{H2AX}$  is known to spread from the actual site of damage to flanking regions of the genome as part of the repair pathway.<sup>21</sup> Therefore, although  $\gamma\text{H2AX}$  is useful as a probe to detect if the line scissors can induce DSBs, it lends

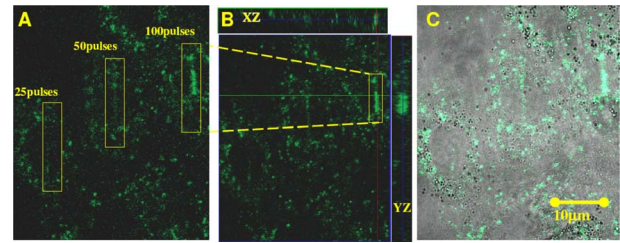


**Fig. 3** DNA damage induced by line scissors. (a) Laser scanning confocal image of HeLa cells stained for  $\gamma\text{H2AX}$  after 25, 50, and 100 pulse exposures. (b) XY, XZ, and YZ cross-sectional view of the DNA damage induced by the line scissors in a HeLa cell. (c) Composite image showing overlay of the fluorescence and phase images.

itself to overestimation of the actual volume of damage induction. To more precisely resolve the zone of DNA damage, parallel experiments were conducted using antibodies against the DSB recognition factor Nbs1. Nbs1 is one of the first recognition factors recruited to DSB damage in mammalian cells and remains largely confined to the actual damage area as compared to  $\gamma\text{H2AX}$ .<sup>21,22</sup> Confocal microscopy analysis of HeLa cells exposed to the line scissors and immunostained for Nbs1 showed a tight linear accumulation (with a cylinder with radius of 2  $\mu\text{m}$ ) of antibody staining corresponding to the region of the linear beam profile exposure [Fig. 4(a)–4(c)]. It may further be noted that the spread of staining also depends on the intensity (or number of pulses) of the laser scissors beam.

In addition, a laser-dose-dependent staining of  $\gamma\text{H2AX}$  and Nbs1 was observed (Fig. 5). Increased localization of  $\gamma\text{H2AX}$  and Nbs1 accumulation is observed with increase in line scissors dose in HeLa cells. Figure 6 shows the comparison of the three methods of applying a laser beam to induce linear patterns of DNA damage in HeLa cells: fast scanning mirror, scanning stage, and line scissors. Fluorescence images of  $\gamma\text{H2AX}$ -Alexa staining in cells exposed to different numbers of laser pulses (same energy/pulse) shows that the line

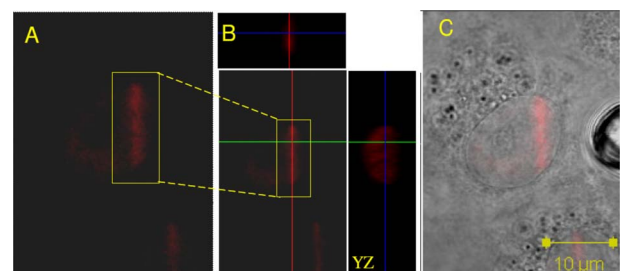


**Fig. 4** DNA repair factor (Nbs1) accumulation in areas of damage induced by line scissors. (a) Laser scanning confocal image of HeLa cells exposed to 150 pulses. (b) XY, XZ, and YZ cross-sectional view of the accumulation of repair factor in areas of DNA damage induced by the line scissors in a CFPAC cell. The green line represents the position at which the XZ plane has been acquired. The red line represents the position at which the YZ plane has been acquired. The blue line represents the XY plane position relative to the XZ and YZ planes. (c) Composite image showing overlay of the fluorescence and phase images. Note that all cells in this image were exposed to 150 pulses to illustrate that the threshold for Nbs1 recruitment is below 150 pulses. (Color online only.)

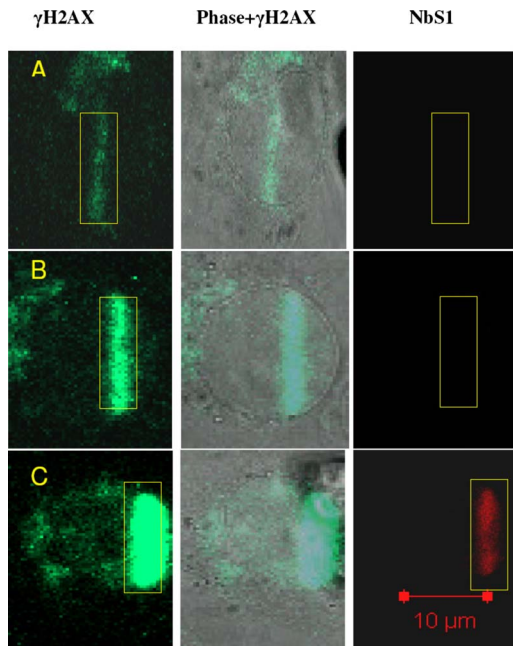


**Fig. 5** Line scissors dose-dependent  $\gamma$ H2AX localization and NbS1 accumulation. Laser scanning confocal images of  $\gamma$ H2AX and NbS1-Alexa staining in CFPAC cells exposed to (a) 50, (b) 100, and (c) 150 pulses. All images are at the same magnification. Scale bar: 10  $\mu$ m. Note that nonlabeled cells in this image were exposed to 100 pulses to further illustrate that the threshold for NbS1 recruitment is between 100 and 150 pulses.

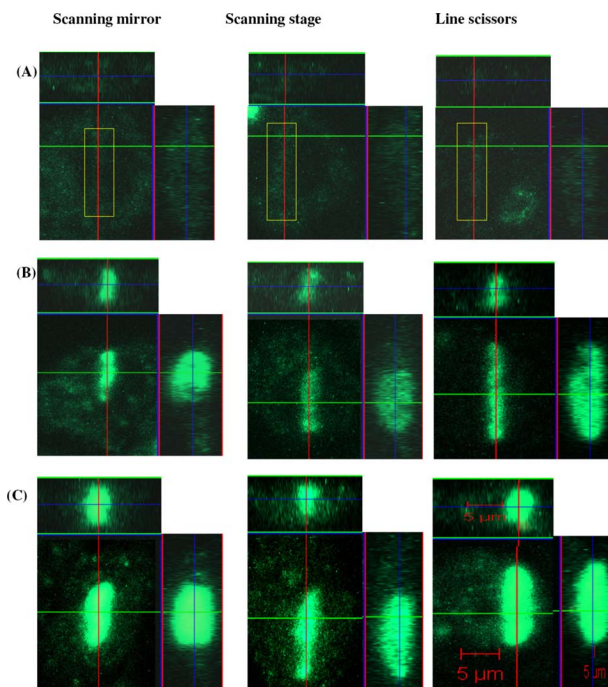


**Fig. 6** Comparison of the scanning mirror, scanning stage, and line scissors induced DNA damage in HeLa cells. Fluorescence images of  $\gamma$ H2AX-Alexa staining in cells exposed to (a) 50, (b) 100, and (c) 150 pulses. Scale bar: 10  $\mu$ m.

scissors is a comparatively simple tool for inducing DNA damage. Since the line scissors requires no dynamic movement of components (such as a scanning stage or an FSM) for laser energy deposition, the linear pattern of damage is more uniform. Additionally, this feature of the line scissors decreases the time necessary to complete damage induction, since deposition of the laser energy is governed only by the repetition rate of the laser (in our case,  $<1$  s for 50 Hz), whereas methods employing repositioning of the stage requires 2 to 4 s per nucleus, and methods requiring repositioning of the scanning mirror required  $\sim 2$  s per nucleus. It should be noted that the application of this approach using solid-state lasers would further increase throughput to subsecond exposure times per nucleus.

#### 4 Conclusion

The linear laser-induced production of damage by the line scissors described in this report utilizes the unique incorporation of a rotatable cylindrical lens in the beam path in combination with a rotatable polarizer for beam attenuation. The level of control over exposed target length and radial orientation of the linearized beam achieved with this optical configuration is a major improvement over existing techniques. This method also has the added benefit of a smooth distribution of energy over the irradiated region. Furthermore, since the full dimension of the exposed region is filled by the beam itself, less time is required to produce damage in each cell, thus greatly increasing the amount of cellular throughput. The line scissors approach should be applicable to other applications such as high-throughput dissection of cells as well as subcellular structures. The incorporation of line tweezers on this system adds microstructure rotation and alignment capabilities<sup>23</sup> that we aim to take advantage of in the future to produce a high-throughput method for the dissection of cells and particles in suspension.

#### Acknowledgments

This work was supported in part by the National Institutes of Health Laser Microbeam and Medical Program (RR01192), the Air Force Office of Scientific Research (FA9550-04-1-0101), and the Beckman Laser Institute Inc. Foundation to M.W.B., and by the National Institutes of Health (CA100710) to K.Y.

#### References

1. *Laser Manipulation of Cells and Tissues*, Methods in Cell Biology, M. W. Berns and K. O. Greulich, Eds., Vol. 82, Elsevier (2007).
2. X. N. Gu, E. R. Macagno, and K. J. Muller, "Laser microbeam axotomy and conduction block show that electrical transmission at a central synapse is distributed at multiple contacts," *J. Neurobiol.* **20**, 422–34 (1989).
3. W. Tao, R. J. Walter, and M. W. Berns, "Laser-transected microtubules exhibit individuality of regrowth, however most free new ends of the microtubules are stable," *J. Cell Biol.* **107**, 1025–35 (1988).
4. E. L. Botvinick, V. Venugopalan, J. V. Shah, L. H. Liaw, and M. W. Berns, "Controlled ablation of microtubules using a picosecond laser," *Biophys. J.* **87**, 4203–4212 (2004).
5. M. W. Berns, R. S. Olson, and D. E. Rounds, "In vitro production of chromosomal lesions with an argon laser microbeam," *Nature (London)* **221**, 74–75 (1969).
6. M. W. Berns, D. E. Rounds, and R. S. Olson, "Effects of laser microirradiation on chromosomes," *Exp. Cell Res.* **56**, 292–298 (1969).
7. M. W. Berns, W. K. Cheng, A. D. Floyd, and Y. Onuki, "Chromo-

- some lesions produced with an argon laser microbeam without dye sensitization," *Science* **171**, 903–905 (1971).
8. S. Kurata, M. Tsukakoshi, T. Kasuya, and Y. Ikawa, "The laser method for efficient introduction of foreign DNA into cultured cells," *Exp. Cell Res.* **162**, 372–378 (1986).
  9. C. L. Limoli and J. F. Ward, "A new method for introducing double-strand breaks into cellular DNA," *Radiat. Res.* **134**, 160–169 (1993).
  10. C. Lukas, J. Falck, J. Bartkova, J. Bartek, and J. Lukas, "Distinct spatiotemporal dynamics of mammalian checkpoint regulators induced by DNA damage," *Nat. Cell Biol.* **5**, 255–260 (2003).
  11. S. Bekker-Jensen, C. Lukas, R. Kitagawa, F. Melander, M. B. Kastan, J. Bartek, and J. Lukas, "Spatial organization of the mammalian genome surveillance machinery in response to DNA strand breaks," *J. Cell Biol.* **173**, 195–206 (2006).
  12. V. Gomez-Godinez, N. M. Wakida, A. S. Dvornikov, K. Yokomori, and M. W. Berns, "Recruitment of DNA damage recognition and repair pathway proteins following near-IR femtosecond laser irradiation of cells," *J. Biomed. Opt.* **12**, 020505-1–3 (2007).
  13. J. S. Kim, T. B. Krasieva, V. J. LaMorte, A. M. R. Taylor, and K. Yokomori, "Specific recruitment of human cohesin to laser-induced DNA damage," *J. Biol. Chem.* **277**, 45149–45153 (2002).
  14. A. Mikhailov, R. W. Cole, and C. L. Rieder, "DNA damage during mitosis in human cells delays the metaphase/anaphase transition via the spindle-assembly checkpoint," *Curr. Biol.* **12**, 1797–1806 (2002).
  15. B. P. Chen, D. W. Chan, J. Kobayashi, S. Burma, A. Asaithamby, K. Morotomi-Yano, E. Botvinick, J. Qin, and D. J. Chen, "Cell cycle dependence of DNA-dependent protein kinase phosphorylation in response to DNA double strand breaks," *J. Biol. Chem.* **280**, 14709–14715 (2005).
  16. H. Misawa, M. Koshioka, K. Sasaki, N. Kitamura, and H. Masuhara, "Three-dimensional optical trapping and laser ablation of a single polymer latex particle in water," *J. Appl. Phys.* **70**, 3829–3835 (1991).
  17. X. Kong, S. K. Mohanty, J. Stephens, J. T. Heale, V. Gomez-Godinez, L. Z. Shi, J. S. Kim, K. Yokomori, and M. W. Berns, "Comparative analysis of different laser systems to study cellular responses to DNA damage in mammalian cells," *Nucleic Acids Res.* **37**, e68 (2009).
  18. T. T. Paull, E. P. Rogakou, V. Yamazaki, C. U. Kirchgessner, M. Gellert, and W. M. Bonner, "A critical role for histone H2AX in recruitment of repair factors to nuclear foci after DNA damage," *Curr. Biol.* **10**, 886–895 (2000).
  19. A. Celeste, O. Fernandez-Capetillo, M. J. Kruhlak, D. R. Pilch, D. W. Staudt, A. Lee, R. F. Bonner, W. M. Bonner, and A. Nussenzweig, "Histone H2AX phosphorylation is dispensable for the initial recognition of DNA breaks," *Nat. Cell Biol.* **5**, 675–679 (2003).
  20. E. P. Rogakou, D. R. Pilch, A. H. Orr, V. S. Ivanova, and W. M. Bonner, "DNA double-stranded breaks induce histone H2AX phosphorylation on serine 139," *J. Biol. Chem.* **273**, 5858–5868 (1998).
  21. E. P. Rogakou, C. Boon, C. Redon, and W. M. Bonner, "Megabase chromatin domains involved in DNA double-strand breaks *in vivo*," *J. Cell Biol.* **146**, 905–915 (1999).
  22. E. Berkovich, R. J. J. Monnat, and M. B. Kastan, "Roles of ATM and Nbs1 in chromatin structure modulation and DNA double-strand break repair," *Nat. Cell Biol.* **9**, 683–690 (2007).
  23. R. Dasgupta, S. K. Mohanty, and P. K. Gupta, "Controlled rotation of biological microscopic objects using optical line tweezers," *Biotechnol. Lett.* **25**, 1625–1628 (2003).